energies

MDPI

Review

Large Eddy Simulation of Film Cooling: A Review

Joon Ahn

School of Mechanical Engineering, Kookmin University, 77 Jeongneung-ro, Seongbuk-gu, Seoul 02707, Republic of Korea; jahn@kookmin.ac.kr

Abstract: Film cooling has dramatically contributed to the performance improvement of gas turbines, as it is a very effective cooling technique for gas turbines. Large eddy simulation (LES) began to be used in the study of film cooling 20 years ago, and meaningful results have been found, but it has not yet been intensively reviewed. In this review paper, we analyze and introduce about 70 papers published on LES of film cooling over the past 20 years. Numerical instability must be overcome, and realistic inflow must be generated to perform LES of film cooling. This review summarizes how the groups that performed LES of film cooling solved these problems. In film-cooling research, the main topics are improving the film-cooling performance by preventing the lift-off of the injectant and the effect of flow conditions on film cooling. In addition, LES has also been conducted extensively on the above two topics, and this review focuses on them. Finally, turbulence statistics of film-cooling flow obtained from LES are introduced, and future challenges of film-cooling LES are predicted.

Keywords: film cooling; large eddy simulation (LES); gas turbine; jet lift-off

Citation: Ahn, J. Large Eddy Simulation of Film Cooling: A Review. *Energies* **2022**, *15*, 8876. https://doi.org/10.3390/en15238876

Academic Editors: Lei Luo, Wei Du and Xiao Liu

Received: 25 October 2022
Accepted: 22 November 2022
Published: 24 November 2022

1. Introduction

A gas turbine is a heat engine that compresses air and burns it with fuel in a combustion chamber to convert high-temperature, high-pressure gas into kinetic energy through a turbine to generate power. The power obtained in this way is used to drive aircraft, ships, generators, and tanks. The gas turbine is a Brayton cycle thermodynamically, and the cycle efficiency increases in proportion to the square root of the turbine inlet total temperature but is limited by material problems [1].

Modern gas turbines operate at turbine inlet total temperatures above the material's allowable limits by extracting some of the compressor air to cool the blades. Compressor air is first supplied to the inside of the blade to cool it, and it is ejected to the surface to additionally protect the blade through film cooling (Figure 1a), which forms an insulating film [2]. Research on gas turbine blade cooling started in the early 1970s, and several books have been published since 2000, as major research achievements have been summarized [3]. Film cooling is one of the most actively studied topics, mentioned by Bunker [4] as a "game changer" for modern gas turbines.

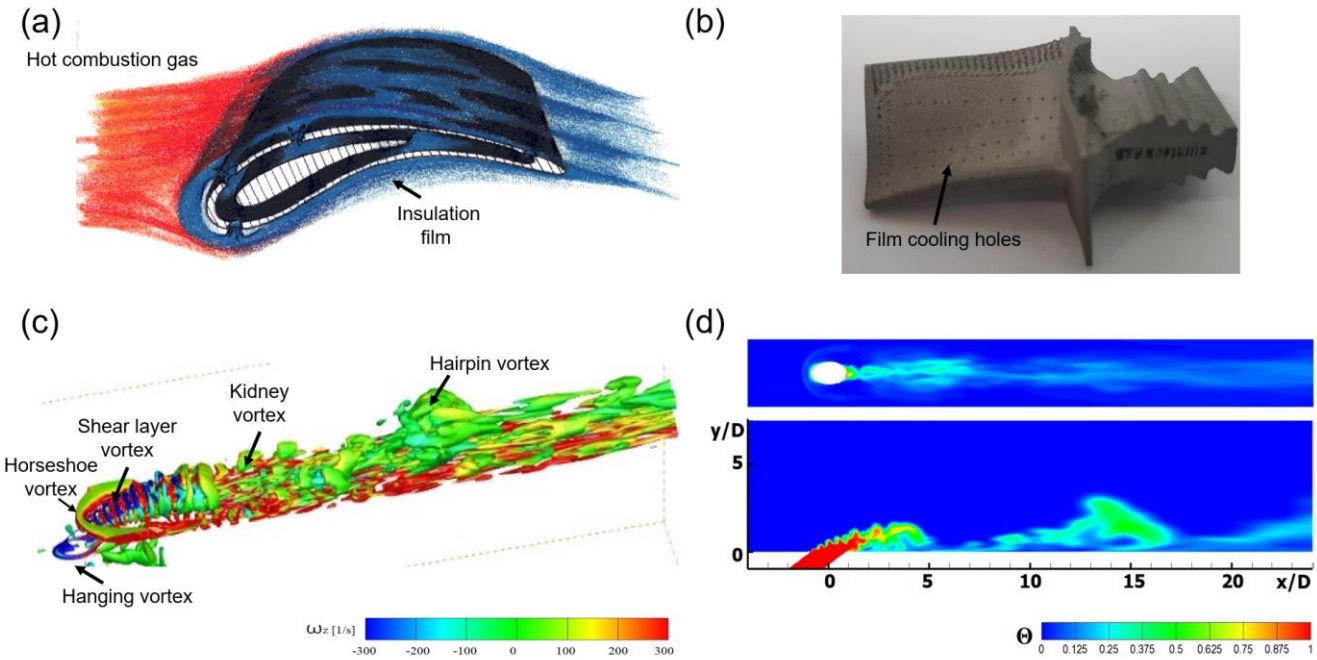

Figure 1. Film cooling of a gas turbine: (**a**) schematic of film cooling, (**b**) gas turbine blades with film-cooling holes installed [5], (**c**) flow structure of the film-cooling jet [6], and (**d**) instantaneous temperature field of film cooling [6].

It is advantageous to inject through a tangential slot on the blade surface to form an insulating film on the surface, but the film-cooling jet is injected through discrete holes to secure mechanical strength, as illustrated in Figure 1b [7]. The jet lift-off occurs from the surface as the inclination angle is created without being tangential to the blade. In addition, when the jet is injected through the holes, the flow becomes complicated three-dimensionally (Figure 1c), increasing mixing with the main flow and lowering the film-cooling performance (Figure 1d). Variables that affect film-cooling performance include the jet/main flow conditions, hole shape, and air-foil geometry [7], and research on these aspects is still ongoing, including LES research.

Gas turbine blades have extreme operating conditions because high-temperature, high-pressure gas is supplied from a combustor. The pressure is 20–40 bar, and the temperature is 1500 °C to 1700 °C. The Reynolds number based on the blade code is about 1 million, and periodic transition occurs. The primary flow turbulence intensity is about 20%, including the wake from the leading blade. The blade-surface heat transfer coefficient is about 2000 W/m^2 K, and the heat flux is 1 million W/m^2 [8]. Therefore, it is challenging to implement all these conditions experimentally, so computational fluid dynamics (CFD) for heat transfer of gas turbines has been continuously attempted [9].

The literature on film-cooling CFD increased from 9 articles in the 1970s to 31 in the 1980s and 147 in the 1990s [10]. During this period, CFD was primarily performed using Reynolds averaged Navier–Stokes (RANS) simulation. Researchers succeeded in reproducing the kidney vortex that occurs in film cooling but could not accurately predict the jet trajectory and mixing, which are essential for film-cooling performance [11]. Until the 1990s, film-cooling CFD adopted a first-order upwind scheme, used a wall function as a wall boundary condition, and lacked grid resolution, which was indicated as the cause of misprediction [12].

In the 2000s, a fully three-dimensional CFD of film cooling was published to solve the above problems [11,12]. These data still overestimate the film-cooling efficiency, but the decreasing downstream trend became similar to that of the experiment. However, the RANS result revealed a limit to be the high blowing ratio at which jet lift-off presented a greater difference from the experiment. For film cooling, various turbulence models were

used for comparison, but no excellent model was found [13], and the effect of improving the prediction according to the model was not evident even in a study with increased grid resolution published 10 years later [14]. When comparing 500,000 to 3 million grids for film-cooling CFD, a grid-independent solution was obtained for over 700,000, but the film-cooling efficiency was over-predicted compared to the experiment [15].

The allowable temperature of Inconel 939, which is often used as a turbine blade material, is about 1200 °C, but it is reported that the blade life is halved if the temperature prediction is 30 °C off [3,7]. In predicting the film-cooling effectiveness of RANS simulation, limitations were exposed in making accurate predictions with the grid resolution or model improvement. Therefore, large eddy simulation (LES), expected to offer more accurate results than RANS simulation, including the unsteady effect, has been attempted since the 2000s.

There were numerical problems, such as inflow generation and stabilization of the convection term, in performing LES of film cooling [16]. In the early 2000s, it took more than a month to analyze film cooling with LES using a supercomputer. Therefore, the turn-around time required for design–prototyping–verification–redesign was too long, making it challenging to apply to the actual design [17]. After overcoming these difficulties, the LES results of film cooling were published in 2003, indicating that centerline film-cooling effectiveness was predicted similarly to the experiment [18]. In addition, the instantaneous flow field was presented, providing valuable information for understanding the film-cooling mechanism.

For the past 20 years, LES studies of film cooling have been steadily published, revealing data that agree better with experiments than RANS simulation and providing information that cannot be obtained with experiments or RANS simulation. Although good review papers have been published on the heat transfer of gas turbines, including film cooling, most are introduced based on the experimental results [19–21], and no review paper has focused on LES.

In this review, about 70 film-cooling LES-related papers published over the past 20 years are introduced and reviewed. First, numerical difficulties are discussed, and how the major research groups that performed film-cooling LES have solved these difficulties are compared. Next, the content of the LES research on film-cooling characteristics according to geometry and flow conditions, which are major research topics of film cooling, are reviewed. Finally, turbulence statistics are reviewed, and future challenges of film-cooling LES are predicted.

2. Numerical Challenges and Comparative Studies

Several computational problems arise when performing LES of film cooling. Ribs are periodically installed in the gas turbine cooling passage; thus, the exit flow is supplied to the computational domain inlet as a periodic condition [22,23]. However, when simulating film cooling, a realistic flow must be created in the inlet at every time step. Film cooling is an external flow; thus, the convection term must be stabilized [24]. In addition, LES requires a subgrid-scale (SGS) model to dissipate turbulent energy within the grid. When a dynamic SGS model with good prediction is used, the model coefficient must be stabilized, and the injection hole and plenum must be included in the computational domain [18]. Table 1 summarizes how the research groups that performed the film-cooling LES solved these problems.

Table 1. Numerical approach by the group that performed LES of film cooling.

Institution (Country)	Software	Convection Term	SGS Model	Inflow Generation
Louisiana State Univ. [18,25–28] (USA)	In house	3rd upwind, WENO	Dynamic, local averaging	Velocity profile
RWTH Aachen [29–33] (Germany)	In house	AUSM	MILES	Rescaling
KIT [34–37] (Germany)	Fluent/ In house	-	Smagorinsky, C_s = 0.1	Rescaling
Virginia Tech. [38–41] (USA)	In house	-	Dynamic	Uniform
ETH [42–45] (Switzerland)	In house	-	ADM	SEM (synthetic eddy)
Denken [46] (Japan)	In house	Bounded central difference	Dynamic	Laminar profile
Penn State Univ. [47–49] (USA)	Fluent	-	Smagorinsky–Lilly	Velocity
Manchester Univ. [50–53] (UK)	Star-CCM+	Bounded central difference	Wall-adapting local eddy viscosity	Uniform
Tsinghua Univ. [54–56] (China)	Fluent	Bounded central difference	Wall-adapting local eddy viscosity	Velocity, Tu = 5%
Nanjing Aviation Univ. [57–62] (China)	Fluent	Bounded central difference	Smagorinsky, C_s = 0.1	Spectral Synthesizer Method
Purdue Univ. [63] (USA)	In house	Beam and Warming	-	Velocity
Stanford Univ. [64,65] (USA)	Vida (Cascade)	-	Vremen	Rescaling
Univ. Texas Austin [66] (USA)	PlasComCM	Pade 6	Wall-adapting local eddy viscosity	Velocity
Harbin Inst. Tech. [67–72] (China)	Fluent	Bounded central difference	Wall-adapting local eddy viscosity	Velocity
Kookmin Univ. [5,6,73–77] (Korea)	Fluent	Bounded central difference	Smagorinsky–Lilly	Velocity
Korea Univ. [78–83] (Korea)	CFX/Fluent	Bounded central difference	Wall-adapting local eddy viscosity	Uniform, Tu = 1%
Shanghai Xiaotong [84–86] (China)	Fluent	Bounded central difference	Wall-adapting local eddy viscosity	Spectral Synthesizer Method
KARI [87,88] (Korea)	CFX	Bounded central difference	Wall-adapting local eddy viscosity	Trip wire/ Cylinder
CEDEX [89] (France)	In house	-	Wall-adapting local eddy viscosity	Velocity

Notes: WENO: weighted essentially non-oscillatory, AUSM: advection upstream splitting method, MILES: monotone integrated large eddy simulation, ADM: approximate deconvolution method.

Film cooling is affected by the outer boundary layer. A thinner boundary layer improves film-cooling effectiveness by suppressing jet lift-off [90]. The boundary layer thickness in the gas turbine blade is similar to the film-cooling hole diameter [90], and a velocity profile is imposed as a boundary condition at the entrance to the computational domain to satisfy this condition in many studies (Table 1).

In addition to the boundary layer thickness, the length scale of the turbulence also affects film cooling [91,92]. A separate turbulent boundary layer simulation is performed for inflow generation to create a more realistic wall turbulence structure, and the inflow is also generated by rescaling the flow of the recycle station [24,93].

In the experiment, a trip wire is used to control the boundary layer thickness [90], and a grid is used to obtain the turbulence intensity of the main flow, similar to that of a real turbine [94]. In imitation of this, Kang et al. performed an LES by including a trip wire [88] or vertical cylinder [87] in the computational domain and obtained an effective distribution more similar to the experiment than when the velocity profile was imposed as an inlet boundary condition.

When analyzing heat transfer in an external flow, numerical instability appears when discretizing the convection term of the energy equation with the standard central difference. This problem can be solved by using the quadratic upstream interpolation for the convective kinematics scheme [95]. For film cooling, a problem of unbounded quadratic interpolation occurs as a coolant with different temperatures is injected through the hole. To solve this problem, most recently published film-cooling LES studies applied a total variation diminishing [96] or a weighted essentially nonoscillatory [97] scheme, which is noted as the bounded central difference.

An SGS model that considers dissipation within the grid is required when performing an LES. The simplest model is to fix the Smagorinsky constant (C_s) as the constant, which has been adopted in some studies. The dynamic model that determines the Smagorinsky constant by detecting changes in the local flow provides improved results [98,99], but the constant tends to become unstable, so appropriate countermeasures are required. The flow is averaged by following the Lagrangian approach [100] and averaging over a local area [101] to solve this problem. The latter case is primarily applied to film cooling. For LES of film cooling, the wall-adapting local eddy viscosity SGS model, which is known to predict asymptotic behavior better than the dynamic model near the wall [102], is the most adopted (Table 1).

Figure 2a compares the centerline efficiency predicted by RANS simulation and LES using the same grid system of 3.6 million when the blowing ratio (M) is 1.0 [6]. The RANS simulation overpredicts the efficiency, although the degree difference depends on the model. The LES presents values similar to the experiment [103].

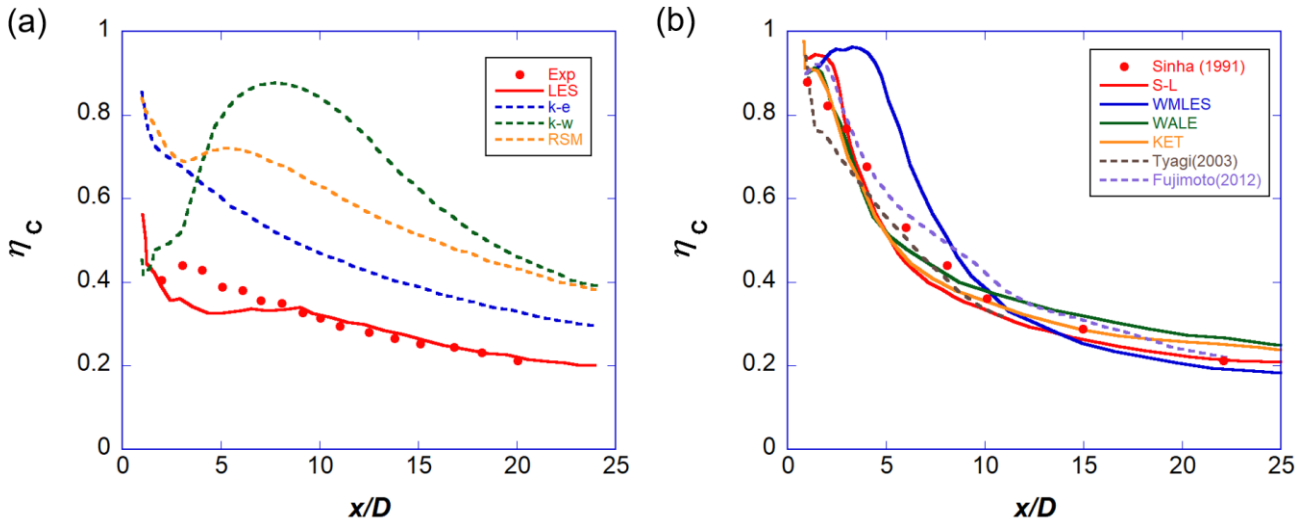

Figure 2. Centerline film-cooling effectiveness: (**a**) LES and RANS simulation data for M = 1.0 [6] and (**b**) LES data for M = 0.5 [5], compared to Sinha [104], Tyagi [18] and Fujimoto [105].

In Figure 2b, the LES was performed with Fluent, and the film-cooling effectiveness according to the SGS model was compared [5]. The wall-adapting local eddy (WALE) viscosity, Smagorinsky–Lilly (S-L), and kinetic energy transport (KET) models exhibited similar results and predicted similar experimental data [104]. Tyagi [18], which adopted a dynamic mixed model and performed in-house code, and Fujimoto [105], which adopted the Smagorinsky–Lilly model and used Open-source Field Operation and Manipulation

(open-FOAM), provided similar results. Only the wall-modeled LES [106] over-predicted the effectiveness compared to other wall-resolved models upstream within $x/D = 10$.

Figure 3 compares the kidney vortex of the film-cooling jet predicted by LES and RANS simulation. In the time-averaged flow field the kidney vortex remains most evident, which is also confirmed by the modal analysis based on proper orthogonal decomposition with LES data [6,27]. Compared to the measurement data using a triple sensor [107], both the LES and RANS simulation are similar to the experiment, but the location where the upward flow occurs near the wall is closer to the experiment in the LES (Figure 3a). By examining the streamwise velocity contour (Figure 3b), it is possible to obtain near-wall data that cannot be measured experimentally through CFD. The LES predicts a jet lift-off greater than that of the RANS simulation, so the low-velocity region (blue) is more widely distributed near the wall.

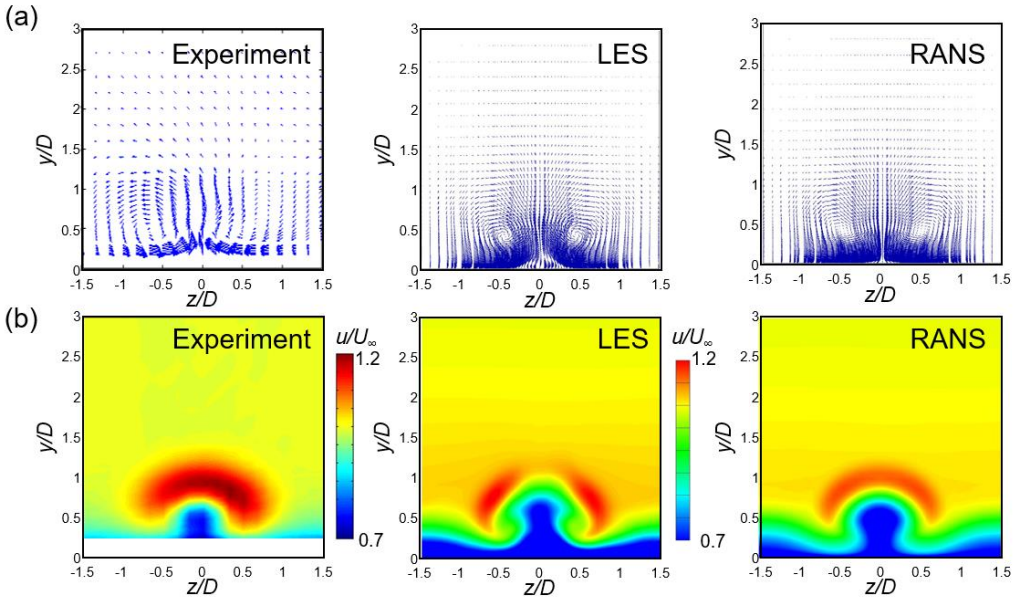

Figure 3. Flow field at x/D = 2.5 for M = 1.0 [5]: (**a**) Cross-stream velocity vectors and (**b**) streamwise velocity contours.

Figure 4 compares the boundary layer temperatures predicted by LES and RANS simulation. Both the LES and RANS simulation predict injectant lift-off or mixing with the main flow, similar to the experiment. However, there is a difference in the temperature near the wall, which is directly related to the film-cooling effectiveness. It is impossible to measure the temperature near the wall using a cold wire; therefore, there are no experimental data [108], and the temperature field obtained from the LES is predicted to cause a more severe jet lift-off than that from the RANS simulation.

In Figure 5, the local effectiveness distributions predicted by LES and RANS simulation are compared with experimental data [108] measured using thermochromic liquid crystal (TLC). At $M = 0.5$ (Figure 5a), the k-ε model and RSM greatly overpredict the effectiveness in the upstream, and a red region appears. In addition, k-ω SST is predicted to match the experiment relatively well upstream, but the mixing with the main flow is weak as it travels downstream. The LES displays a distribution similar to the experiment as a whole.

In $M = 1.0$ (Figure 5b), as injectant reattachment occurs, regions are observed with low effectiveness near $x/D = 1$ and high effectiveness at $3 < x/D < 5$ in the experimental data. Moreover, the RANS simulation does not predict these characteristics in all three compared models. The LES similarly predicts the effectiveness distribution using the lift-off and reattachment observed in the experiment.

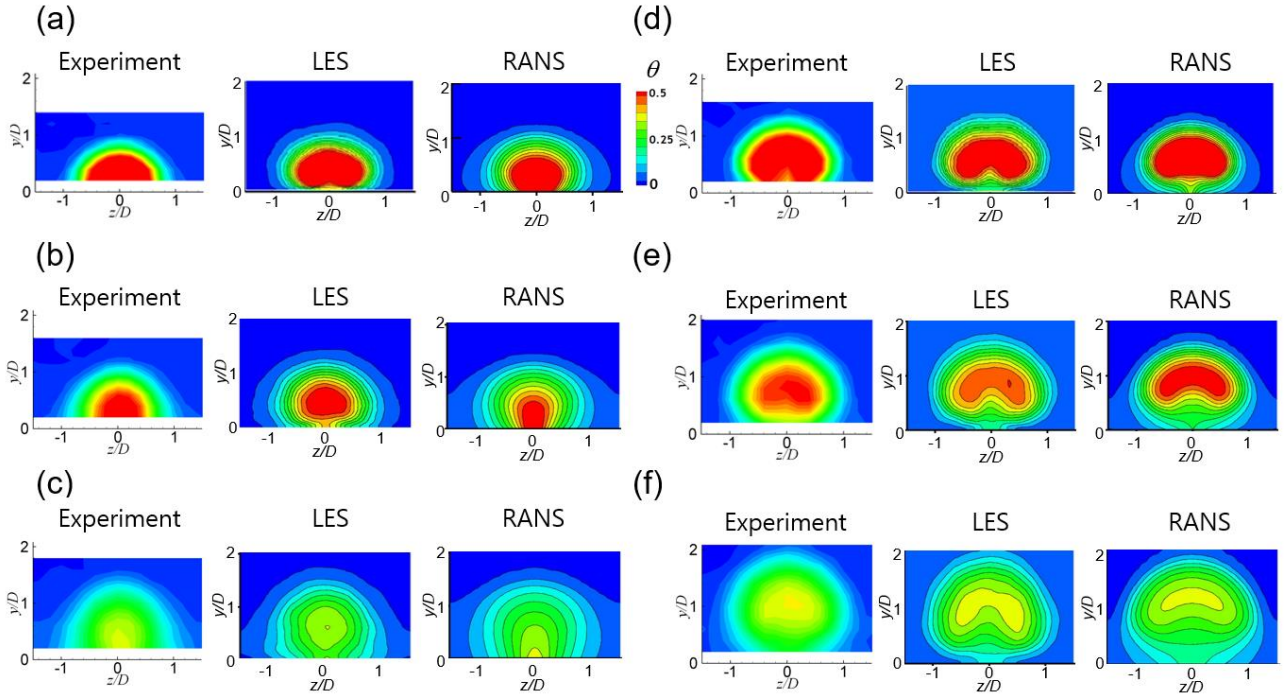

Figure 4. Boundary layer temperature distributions in the streamwise normal planes [5]: (**a**) $x/D = 2.5$, $M = 0.5$; (**b**) $x/D = 5.0$, $M = 0.5$; (**c**) $x/D = 10.0$, $M = 0.5$; (**d**) $x/D = 2.5$, $M = 1.0$; (**e**) $x/D = 5.0$, $M = 1.0$; and (**f**) $x/D = 10.0$, $M = 1.0$.

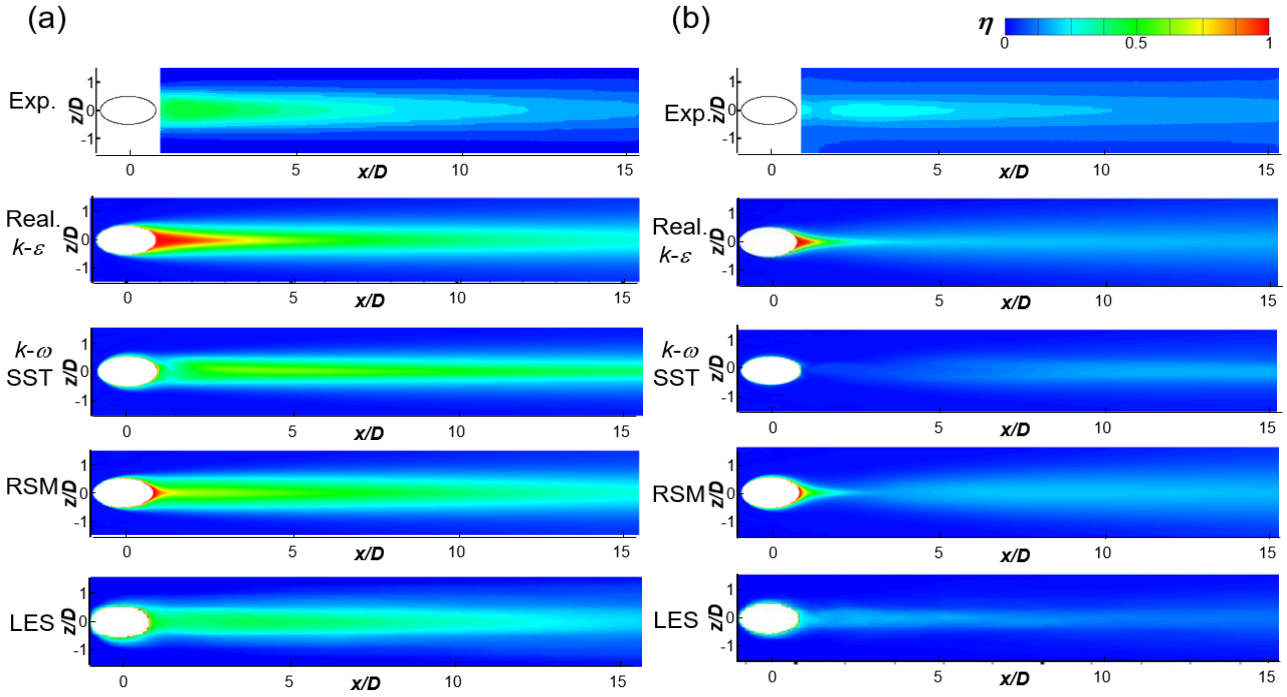

Figure 5. Local adiabatic film-cooling effectiveness distributions [5]: (**a**) $M = 0.5$ and (**b**) $M = 1.0$.

3. Hole and Injection Geometry Studies

Geometrical parameters and flow conditions influence film cooling. Geometrical parameters can be divided into injection geometry and blade geometry [7]. Blade geometry is a curvature effect. In the convex surface, downstream effectiveness is lower than that of the flat plate, and in the concave surface, a re-increase of effectiveness is observed [109]. In LES of film cooling, studies that adopt air-foil geometry [51,52,57,58] or analyze film

cooling [38–40] at the leading edge have been published. However, the blade geometry does not significantly affect film cooling near the hole downstream, where the main flow strongly interacts with film cooling, so many LES studies focus on the hole or injection geometry.

Hole geometry has been actively studied to solve the lift-off problem of the inclined jet. If the blowing ratio is lowered, lift-off can be reduced, but under unsteady flow conditions the main flow may be injected into the cooling hole. The goal is to prevent lift-off at the blowing ratio where injection does not occur; therefore, the passive technique of deforming the shape or installing a fixed device has primarily been studied. Recently, an active technique to control injection according to flow conditions has been proposed [19].

The most representative hole geometry is an expanded hole, which narrows the inlet to prevent injection and expands at the outlet to prevent lift-off. In addition, reducing the interaction with the main flow makes it possible to lower the heat transfer coefficient and suppress mixing with the main flow [4].

The shaped hole expands the hole in the spanwise direction [110], streamwise direction [111], or both [112,113] at the exit, as depicted in Figure 6. The expanded hole can be applied to actual turbine blades using electro-discharge machining [4], and additive manufacturing has also been actively considered [21]. Bell et al. [114] compared the film-cooling effectiveness for several expansion holes and found better film-cooling performance when the fan-shaped hole was at a compound angle rather than a simple angle compared to the forward expansion hole. Film cooling of shaped holes, including fan-shaped holes, is the most recently conducted and published topic for LES [55,58,65,66,75,79–85,87,88].

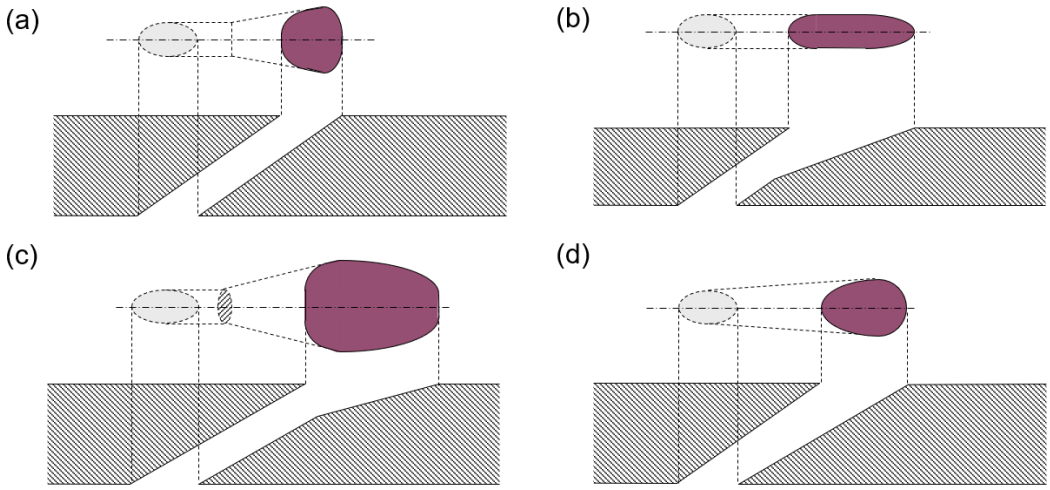

Figure 6. Various expansion types of shaped holes: (**a**) lateral expansion [110], (**b**) forward expansion [111], (**c**) forward-lateral expansion [112], and (**d**) conical expansion [113].

In Figure 7, RANS simulation and LES were performed for film cooling by adopting a forward expansion hole and were compared with film-cooling effectiveness distributions [115] measured using TLC. At a simple angle (Figure 7a,b), the RANS result overpredicts the effectiveness at the centerline compared to the experiment and predicts less mixing with the main flow as it progresses downstream. The LES predicts quantitative effectiveness and downstream characteristics, similarly to the RANS simulation.

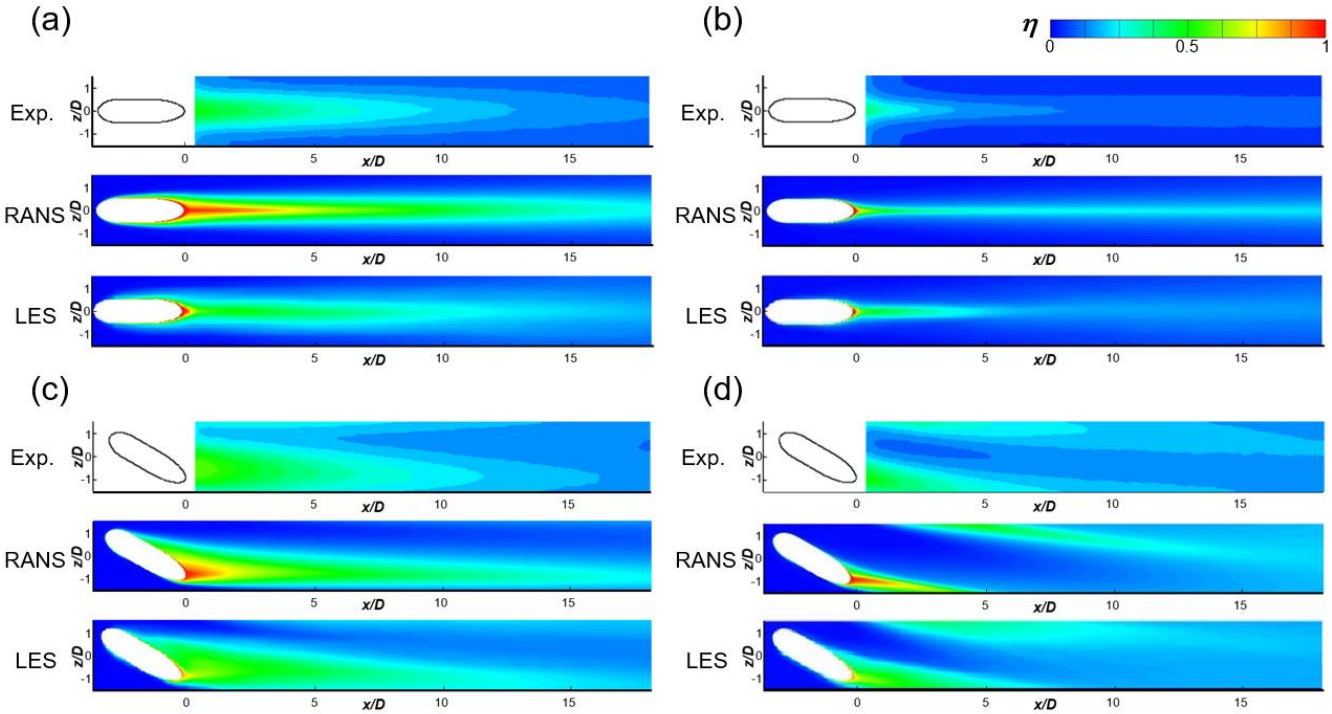

Figure 7. Local adiabatic film-cooling effectiveness distributions with the forward expansion hole [72]: (**a**) simple angle, $M = 0.5$; (**b**) simple angle, $M = 1.0$; (**c**) compound angle, $M = 0.5$; and (**d**) compound angle, $M = 1.0$.

At the compound angle (Figure 7c,d), the film-cooling efficiency between holes is improved, and CFD predicts this. Moreover, the RANS simulation predicts the mixing with the main flow and lateral spread to be smaller than the experimental ones, but the LES predicts them to be closer to the experimental results. Accurate prediction of the local effectiveness distribution is crucial for shape optimization, which can be confirmed in the following example.

Figure 8 compares the shapes obtained by optimizing the fan-shaped film-cooling hole with RANS simulation [116,117], experiments using pressure-sensitive paint (PSP) [118,119], and LES [79]. The shape reduces forward expansion and increases lateral expansion compared to the reference. However, the optimal shape obtained by the LES is remarkably similar to that obtained by the experiment, but the shape obtained by the RANS simulation is somewhat different.

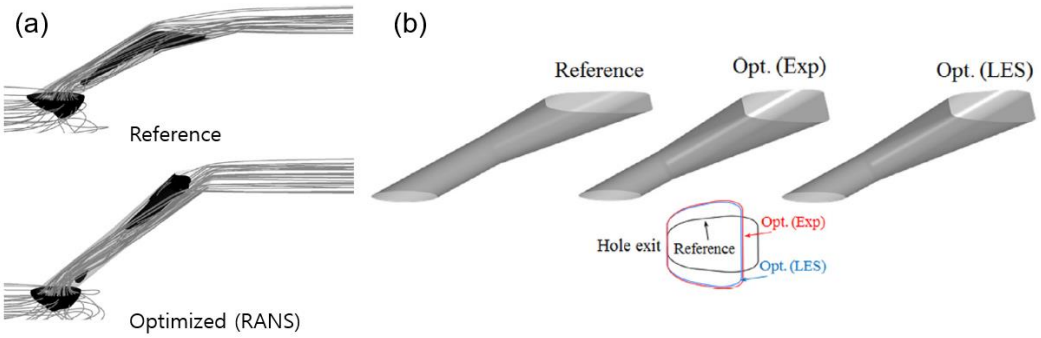

Figure 8. Shape optimization of fan-shaped holes: (**a**) RANS-based optimization [117] and (**b**) experiment- and LES-based optimizations [79].

The combined-hole and shaped-hole configurations have recently attracted attention as techniques to solve jet lift-off [20]. The combined hole uses the idea of suppressing jet lift-off by locating the downward flow of the vortex generated by the film-cooling jet in

the adjacent or downstream hole. Sister holes, anti-vortex holes, and double holes were assessed, and after the shape was proposed using RANS simulation, the shape was often validated through experiments [20].

Wu et al. [120] measured the film-cooling effectiveness of triple holes using TLC. Triple holes improved film-cooling effectiveness compared to single holes, and jet lift-off did not significantly occur even at high blowing ratios, consistent with the LES results in Figure 9. The principle and effect of anti-vortex holes are largely similar to those of triple holes [20], and the results of LES have not yet been reported.

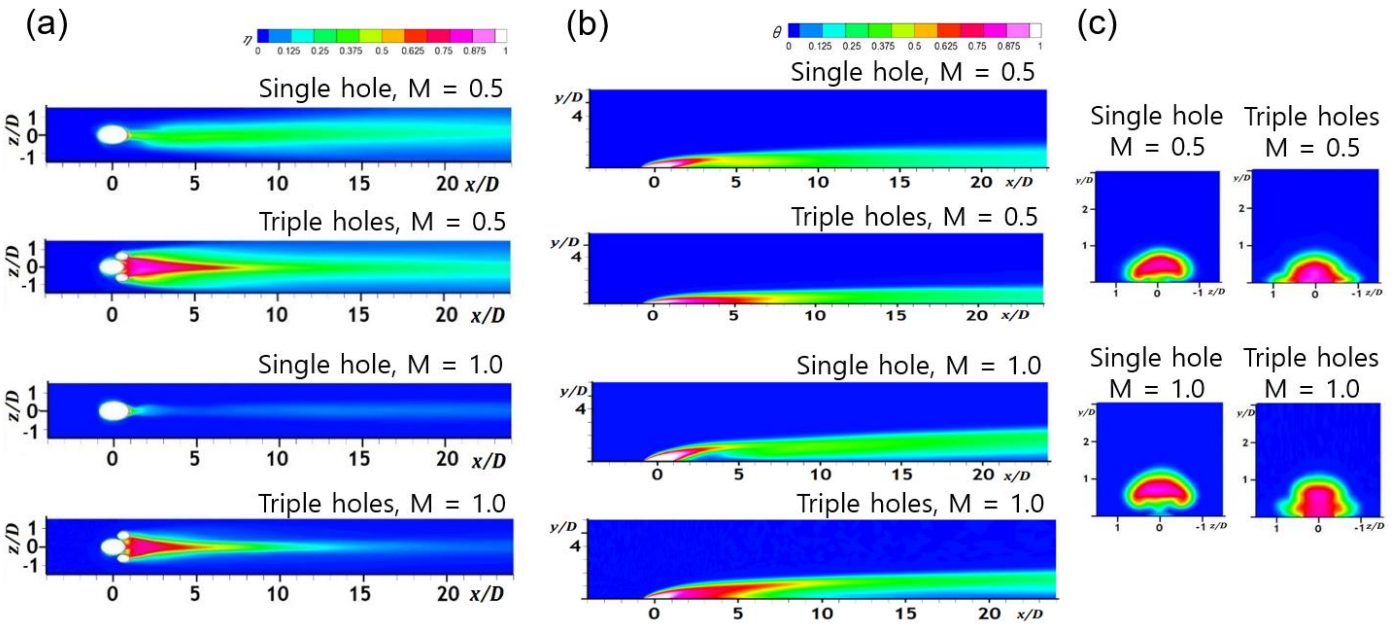

Figure 9. Film cooling with triple holes [73]: (**a**) film-cooling effectiveness, (**b**) temperature fields at $z/D = 0$, and (**c**) temperature fields at $x/D = 2.5$.

There is also a double-jet hole in the combined hole, which adopts a compound angle and arranges in two rows so that the downward flow of the upstream hole is located at the downstream hole exit, suppressing lift-off [121]. Film-effectiveness distribution [122] measured by PSP recently appeared similar to TLC data [121], and a similar distribution was maintained even under the condition of a density ratio of 1.5, which is close to an actual gas turbine (Figure 10a). LES [43,45] can also consider the density ratio, similar to the PSP measurement method, and predict double-jet film cooling similarly to the experiment (Figure 10b).

In addition to the hole shape mentioned so far, the effects of passive devices [19] that control the lift-off of film cooling, such as the trench or delta wing vortex, are also being studied with LES. The trench occurs naturally in a mask that prevents the clogging of film-cooling holes when a thermal barrier coating is applied to blades, but it can also alleviate jet lift-off and increase film-cooling performance depending on the thickness [123]. Moreover, some researchers [60,61] have performed LES of film cooling that includes the trench on the air-foil surface. Another study [61] proposed a serrated trench. In addition, some researchers [67,68] have performed LES of film cooling with a trench and presented changes in the shear layer vortex in the trench. Further, several researchers [69–72] made a vortex pair with a delta wing and studied the lift-off characteristics of a film-cooling jet with single-row and two-row structures using LES.

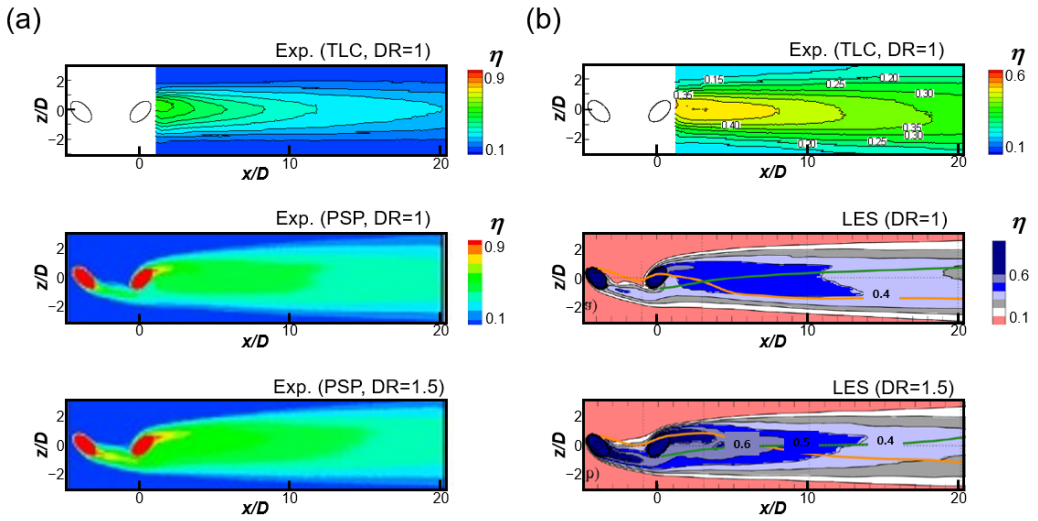

Figure 10. Double-jet film-cooling effectiveness distributions: (**a**) $M = 0.5$ and (**b**) $M = 1.0$.

4. Free-Stream and Coolant Flow Studies

In film cooling, the geometry of the hole and blade and the conditions of the free stream and injectant have considerable influence [7]. The free stream supplied from the combustor is a complex unsteady flow, and the following four major unsteadiness aspects are discussed [124]. First, strong turbulence occurs in the combustor, and then a shock wave occurs as the transonic flow occurs. In addition, the axial turbine is composed of a rotor and stator. A wake occurs at the upstream blade, affecting the downstream blade, and pressure pulsation depends on the relative position of the rotor and stator.

When testing the wake using the upstream rotor, it is supplied by a circular cylinder wake generator [125] and promotes the mixing of the main flow and the film-cooling jet, reducing the film-cooling effectiveness. In particular, in the vicinity of the leading edge where the stagnation line exists, the transition to turbulence is also of interest, and LES results have also been published [126,127]. In one study [126], a wake was generated from the combustor wall by including a hexahedral structure near the computational domain inlet, and another study [127] simulated the wake occurring in the rotor by moving the cylinder as in the experiment. Both studies analyzed the interaction of the flow structure occurring in the wake and film-cooling jet as an instantaneous flow field and discussed the mechanism through which the film-cooling performance deteriorated at a specific location or periodically.

Free-stream turbulence from the combustor also has unsteadiness that affects film cooling. The turbulence intensity can be up to 20%, and the integral length scale is about the hole diameter [128]. In experiments, turbulence is primarily generated using a grid [94], but jet arrays are also used to obtain high-intensity turbulence similar to the combustor exit [128]. One study [44] performed LES considering free-stream turbulence to be a synthetic vortex method and obtained film-cooling effectiveness closer to the experiment than in [42], which did not include inflow turbulence. Another study [87] created free-stream turbulence by including vertical cylinder arrays in the domain, as depicted in Figure 11, similar to grid turbulence, and obtained film-cooling effectiveness similar to the experiment.

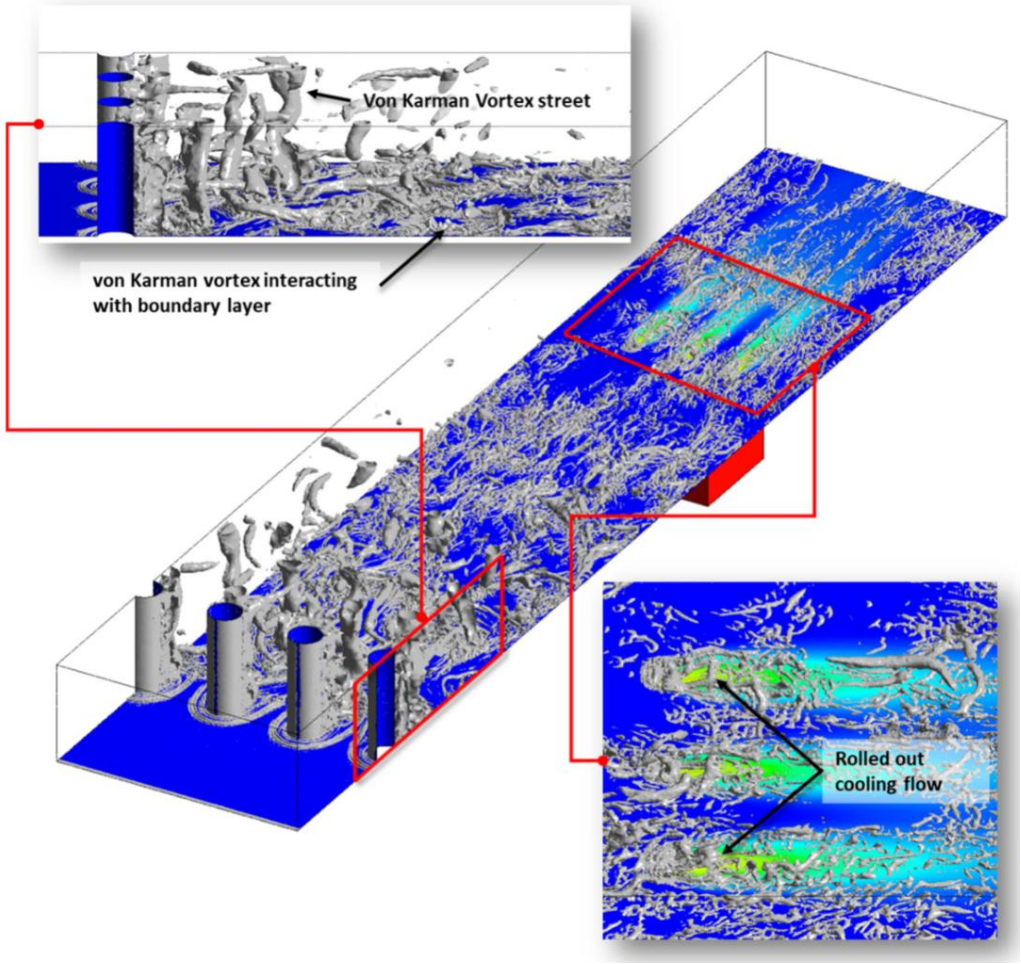

Figure 11. Vortex structures of shaped-hole film cooling supplied with free-stream turbulence created using a vertical cylinder [87].

An experiment on the effect of shock waves on film cooling was conducted in a transonic wind tunnel [129]. When the shock wave passes over the film-cooling hole, the static pressure fluctuates and deteriorates the film-cooling performance. Another study [33] revealed that film effectiveness could be reduced by 30% by performing LES with an oblique shock wave. One study [66] found that the film-cooling effect of the shaped hole was made asymmetrical with the shock wave through the LES at a high Mach number.

Although pressure pulsation occurs at the hole exit, even with the shock wave mentioned above, periodic pressure pulsation occurs due to the rotor–stator interaction, even without a shock wave [124]. Moreover, another researcher [130] demonstrated that the film-cooling performance deteriorated as the injection was made intermittently using bulk-flow pulsation. Another study [76] performed LES and unsteady RANS simulation for film cooling with flow pulsation and compared them to the experimental results in [131], as indicated in Figure 12.

As previously discussed, in the absence of pulsation, the RANS simulation overpredicts film-cooling effectiveness, but the LES predicts it well (Figure 12a). When pressure pulsation occurs in the main flow (Figure 12b), the RANS simulation does not predict that film cooling is greatly reduced by pulsation, but the LES predicts this well.

Figure 12c,d compare the boundary layer temperature obtained by LES and RANS simulation with cold wire data [131]. The cold wire does not provide data near the wall; thus, an accurate comparison is difficult, but when there is no pulsation (Figure 12c), the LES and RANS simulation similarly predict injectant dilution by the main flow. However, when pulsation is applied (Figure 12d), the RANS simulation fails to predict the mixing.

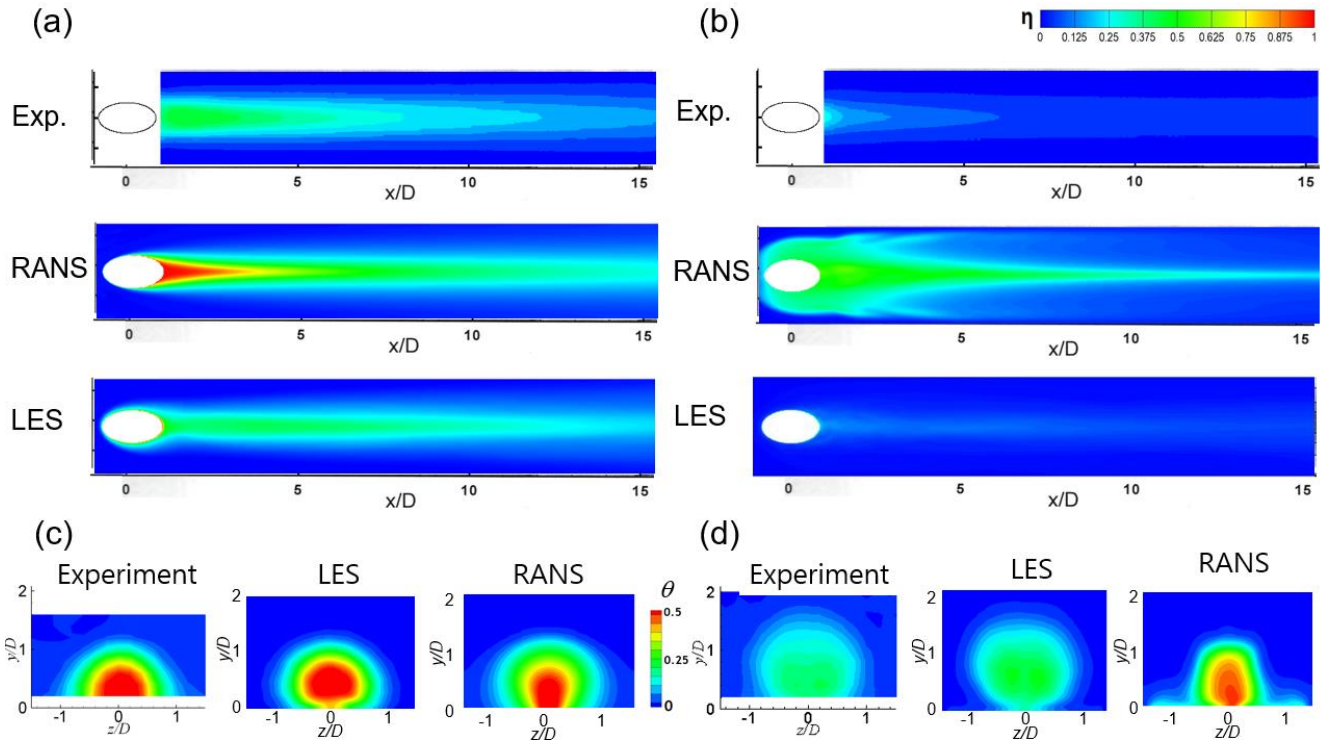

Figure 12. Film cooling with bulk-flow pulsation for $M = 0.5$ [76]: (**a**) effectiveness without pulsation, (**b**) effectiveness with pulsation, (**c**) boundary layer temperature at $x/D = 2.5$ without pulsation, and (**d**) boundary layer temperature at $x/D = 2.5$ with pulsation.

Although the boundary layer thickness and turbulence characteristics of the main flow discussed above affect film cooling, the vortex embedded in the boundary layer also affects film cooling [132]. When a longitudinal vortex with a size similar to the boundary layer thickness exists, it has a substantial effect: downward flow inhibits lift-off, and upward flow promotes it [132]. In LES studies, the injectant was controlled by artificially creating a vortex pair about the boundary layer thickness with a delta wing [69–72].

In addition to the flow conditions of the free stream discussed so far, the conditions of the injectant also affect film cooling. A representative parameter is the density ratio. In the experiment, a gas heavier than air, such as CO_2, is supplied as coolant [133], or the coolant is cooled to a cryogenic temperature [104] so that the density ratio is similar to that of a gas turbine. Recently, a density ratio similar to that of a gas turbine was realized by matching the density of tracer gas, as PSP is frequently used to measure film-cooling effectiveness [134]. In the LES, the density ratio was reflected by a conservative formulation based on the mass flux, and the blowing ratio was an appropriate parameter to determine the performance of film cooling when the density ratio was considered [30,31].

In many experiments, the injectant is supplied through the plenum, but the actual cooling passage of the gas turbine blade has a complicated structure, so it is necessary to study the supply geometry [135], and LES is also actively used. Another study [26] assessed film cooling according to the hole length and the flow direction in the plenum with LES and discussed the flow change inside the hole, which is difficult to measure experimentally. In [82], the effect of supply orientation on shaped-hole film cooling with LES was observed, and another study [136] presented the effect of generating swirl flow in the plenum as LES data.

5. Turbulence Studies

The film-cooling performance is affected by jet lift-off and mixing with the main flow, and turbulence intensity or scale greatly influences them [137]. In the data published so

far, the time-averaged flow field and boundary layer temperature can be predicted to an extent using RANS simulation, but the turbulence intensity was hardly predicted with RANS simulation [6,23]. Reynolds stresses have several independent components and are challenging to measure because they require a fast response, so the role of LES is expected.

Experimental data on the turbulence quantities of film-cooling flow are rare compared to film-cooling effectiveness or heat transfer, and data on temperature fluctuations and turbulent heat flux required for heat transfer analysis are scarce [137]. One study [137] presented Reynolds stress and turbulent heat flux measurements at the center plane ($z/D = 0$) using laser Doppler velocimetry and cold wire. Another study [138] published the Reynolds stress in a horizontal plane with a height of $y/D = 0.5$ using magnetic resonance velocimetry. Other studies [139,140] have measured Reynolds stress using particle image velocimetry in the streamwise normal plane (yz-plane) of the film-cooling jet.

With LES, information about the turbulence of the film-cooling flow can be obtained, and information can be obtained near the wall, which is difficult to measure with a triple sensor or particle velocimetry. In Figure 13, the turbulence components generated in the film-cooling flow were calculated using LES and compared with the experiment [5]. Experiments and LES predictions are qualitatively and quantitatively very similar, and LES provides information near the wall where no measurement data are available. The behavior of u_{rms} and w_{rms} near the wall is similar, but v_{rms} converges to a minimal value.

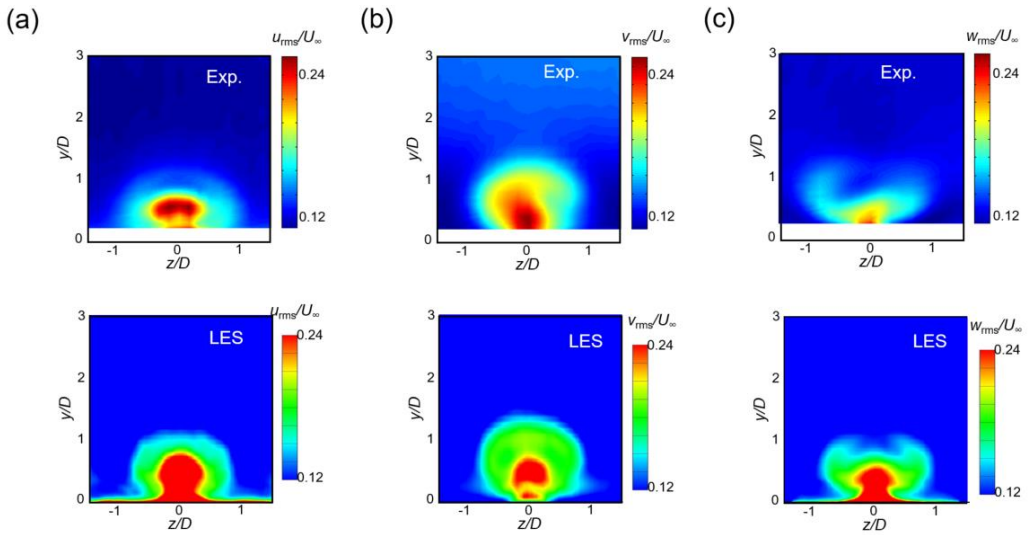

Figure 13. Turbulence intensities of a film-cooling jet at $x/D = 2.5$ [5]: (**a**) u_{rms}, (**b**) v_{rms}, and (**c**) w_{rms}.

In Figure 14 [77], the Reynolds stress obtained through LES in three measurement planes was compared with experimental data [138,141]. Compared to the turbulence intensities in Figure 13, the Reynolds stress obtained by LES is slightly different from the experimental data, but the overall distribution is predicted to be similar. In particular, in Figure 14a,c, the near-wall data that could not be measured experimentally can be observed in the LES.

Figure 15 compares the temperature fluctuations of simple-angle and compound-angle film cooling obtained through LES. When there is no flow pulsation (Figure 15a), there is a region with weak fluctuations in the jet core that has a vastly different distribution from the turbulence intensities in Figure 13. In Figure 15b, when pulsation is applied to the free stream, the temperature fluctuation increases in the jet core.

The high-order statistics and turbulent heat flux are particularly important information for understanding heat transfer mechanisms and developing turbulent heat transfer models [142]. One study [143] found that the turbulent Prandtl number (Pr_t) had a profound influence on the film-cooling simulation results, and in the measurement results of another study [137] Pr_t ranged from 0.5 to 2, revealing a local four-fold difference. The Pr_t

distribution presented by [142] as the LES result was highly three-dimensional. Recently, studies have been published to predict the turbulent heat flux or Pr_t in film cooling through machine learning based on LES data [144,145].

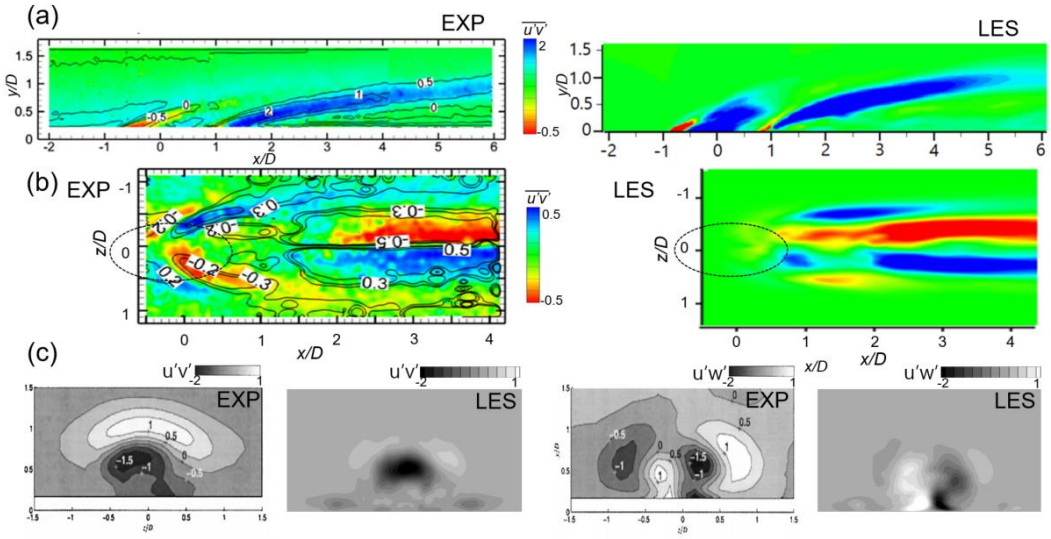

Figure 14. Reynolds stress contours [77]: (**a**) at $z/D = 0$, (**b**) at $y/D = 0.5$, and (**c**) at $x/D = 2.5$.

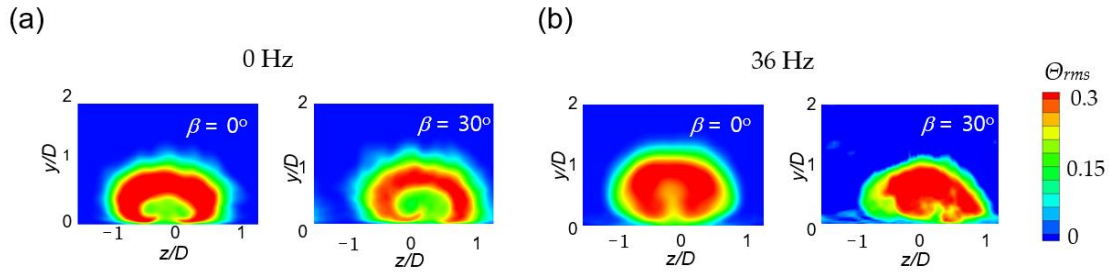

Figure 15. Temperature fluctuations at $x/D = 2.5$ [77]: (**a**) $M = 0.5$, steady; and (**b**) $M = 0.5$ with bulk-flow pulsation.

6. Summary and Future Prospects

In this review paper, about 70 articles related to film cooling in LES papers were reviewed. The numerical difficulties and methods of overcoming the problems that appeared in the process of performing LES of film cooling were compared. The complex flow structure of film cooling was identified through the instantaneous flow field obtained from LES, and the film-cooling performance, which could not be predicted with RANS simulation, was successfully predicted. LES has been actively used to determine the geometry that improves film-cooling performance, and shape optimization results similar to those of the experiment were obtained. According to the results of the recently published research, the following studies are expected to continue in the future.

1. The increase in computing power over the past two decades has made it possible to solve increasingly complex problems. In the future, LES of film cooling will apply more realistic geometry and flow conditions close to gas turbine operating conditions, and studies will expand to conjugate heat transfer including conduction.
2. Recently, with the help of additive manufacturing, more complex shapes can be realized in film cooling [21], and LES can be used to discover and optimize new shapes.
3. Film-cooling research has been focused on effectiveness, and research on the heat transfer coefficient has been lacking. The insulation effect of film cooling is inversely proportional to the heat transfer coefficient, and when the blowing ratio or unsteadi-

ness is large, film-cooling performance is substantially affected [146]. Thus, LES can make a good contribution to heat transfer predictions in the future.

4. As LES can provide turbulence statistics and considerable instantaneous flow field and temperature field data, attempts to link it with data-driven engineering, including machine learning, have recently been made. It is expected that such studies will be conducted in the future.

Funding: This research received no external funding.

Data Availability Statement: Data is contained within this article.

Conflicts of Interest: The author declares no conflict of interest.

Nomenclature

Cs	Smagorinsky eddy viscosity constant
D	hole diameter
L	hole length
M	blowing ratio = $(\rho_C U_C)/(\rho_G U_G)$
Pr_t	turbulent Prandtl number
U	flow velocity [m/s]
u	streamwise velocity component [m/s]
v	wall-normal velocity component [m/s]
w	spanwise velocity component [m/s]
x	streamwise coordinate
y	wall-normal coordinate
z	spanwise coordinate
Greek symbols	
β	orientation angle angle between the streamwise direction and projected injection vector on the x–z plane
η	adiabatic film-cooling effectiveness = $\frac{(T_G - T_{aw})}{T_G - T_C}$
η_m	spanwise-averaged film-cooling effectiveness
ρ	density [kg/m^3]
Θ	dimensionless temperature = $\frac{(T_G - T)}{T_G - T_C}$
Subscripts	
C	coolant
G	mainstream gas
m	spanwise-averaged
rms	root mean squared
Abbreviations	
DR	density ratio
LDV	laser doppler velocimetry
LES	large eddy simulation
PSP	pressure sensitive paint
RANS	Reynolds-averaged Navier–Stokes simulation
TLC	thermochromic liquid crystal
PIV	particle image velocimetry

References

1. Lakshminarayana, B. *Fluid Dynamics and Heat Transfer of Turbomachinery*; Wiley: Hoboken, NJ, USA, 1996; pp. 315–322.
2. Goldstein, R.J. Film cooling. In *Advances in Heat Transfer*; Elsevier: Amsterdam, The Netherlands, 1971; Volume 7, pp. 321–379.
3. Han, J.C. Advanced cooling in gas turbines 2016 Max Jakob Memorial Award Paper. *ASME J. Heat Transf.* **2018**, *140*, 113001. [CrossRef]
4. Bunker, R.S. A review of shaped hole turbine film-cooling technology. *ASME J. Heat Transf.* **2005**, *127*, 441–453. [CrossRef]
5. Baek, S.I.; Ahn, J. Large eddy simulation of film cooling involving compound angle holes: Comparative study of LES and RANS. *Processes* **2021**, *9*, 198. [CrossRef]

6. Baek, S.I.; Ahn, J. Large eddy simulation of film cooling with bulk flow pulsation: Comparative study of LES and RANS. *Appl. Sci.* **2020**, *10*, 8553. [CrossRef]
7. Bogard, D.; Thole, K. Gas turbine film cooling. *J. Propul. Power* **2006**, *22*, 249–270. [CrossRef]
8. Han, J.C. Fundamental gas turbine heat transfer. *ASME J. Thermal Sci. Eng. Appl.* **2013**, *5*, 021007. [CrossRef]
9. Han, J.C. Recent development in turbine blade film cooling. *Int. J. Rotating Mach.* **2001**, *7*, 21–40. [CrossRef]
10. Kercher, D.M. A film-cooling CFD bibliography: 1971–1996. *Int. J. Rotating Mach.* **1998**, *4*, 61–72. [CrossRef]
11. Walters, D.K.; Leylek, J.H. Impact of film-cooling jets on turbine aerodynamic losses. *ASME J. Turbomach.* **2000**, *122*, 537–545. [CrossRef]
12. McGovern, K.T.; Leylek, J.H. A detailed analysis of film cooling physics: Part II—Compound-angle injection with cylindrical holes. *ASME J. Turbomach.* **2000**, *122*, 113–121. [CrossRef]
13. Ferguson, J.D.; Walters, D.K.; Leylek, J.H. Performance of turbulence models and near-wall treatments in discrete jet film cooling simulations. In Proceedings of the ASME Turbo Expo 1998, Stockholm, Sweden, 2–5 June 1998; p. V004T09A077.
14. Harrison, K.L.; Bogard, D.G. Comparison of RANS turbulence models for prediction of film cooling performance. In Proceedings of the ASME Turbo Expo 2008, Berlin, Germany, 9–13 June 2008; pp. 1187–1196.
15. Na, S.; Shih, T. Increasing adiabatic film cooling effectiveness by using an upstream ramp. *J. Heat Transf.* **2007**, *129*, 464–471. [CrossRef]
16. Karagozian, A.R. The jet in crossflow. *Phys. Fluids* **2014**, *26*, 101303. [CrossRef]
17. Kumar, S.; Amano, R.S. An investigation in the numerical approach to solve the heat transfer phenomenon in gas turbine. *ASME J. Energy Resour. Technol.* **2021**, *143*, 080805. [CrossRef]
18. Tyagi, M.; Acharya, S. Large eddy simulation of film cooling flow from an inclined cylindrical jet. *ASME J. Turbomach.* **2003**, *125*, 734–742. [CrossRef]
19. Zhang, J.; Zhang, S.; Wang, C.; Tan, X. Recent advances in film cooling enhancement: A review. *Chin. J. Aeronaut.* **2020**, *33*, 1119–1136. [CrossRef]
20. Zhu, R.; Zhang, G.; Li, S.; Xie, G. Combined-hole film cooling designs based on the construction of antikidney vortex structure: A review. *J. Heat Transf.* **2021**, *143*, 030810. [CrossRef]
21. Dutta, S.; Kaur, I.; Singh, P. Review of film cooling in gas turbines with an emphasis on additive manufacturing-based design evolutions. *Energies* **2022**, *15*, 6968. [CrossRef]
22. Ahn, J.; Choi, H.; Lee, J.S. Large eddy simulation of flow and heat transfer in a channel roughened by square or semicircle ribs. *ASME J. Turbomach.* **2005**, *127*, 263–269. [CrossRef]
23. Tafti, D.K. Large-eddy simulation for turbulent heat transfer. *ASME J. Thermal Sci. Eng. Appl.* **2013**, *5*, 021001. [CrossRef]
24. Lund, T.S.; Wu, X.; Squires, K.D. Generation of turbulent inflow data for spatially-developing boundary layer simulations. *J. Comp. Phys.* **1998**, *140*, 233–258. [CrossRef]
25. Muldoon, F.; Acharya, S. DNS study of pulsed film cooling for enhanced cooling effectiveness. *Int. J. Heat Mass Transf.* **2009**, *52*, 3118–3127. [CrossRef]
26. Acharya, S.; Leedom, H.D. Large eddy simulations of discrete hole film cooling with plenum inflow orientation effects. *ASME J. Heat Transf.* **2013**, *135*, 011010. [CrossRef]
27. Kalghatgi, P.; Acharya, S. Modal analysis of inclined film cooling jet flow. *ASME J. Turbomach.* **2014**, *136*, 081007. [CrossRef]
28. Kalghatgi, P.; Acharya, S. Improved film cooling effectiveness with a round film cooling hole embedded in a contoured crater. *ASME J. Turbomach.* **2015**, *137*, 101006. [CrossRef]
29. Guo, X.; Schröder, W.; Meinke, M. Large-eddy simulations of film cooling flows. *Comput. Fluids* **2006**, *35*, 587–606. [CrossRef]
30. Renze, P.; Schröder, W.; Meinke, M. Large-eddy simulation of film cooling flows with variable density jets. *Flow Turbul. Combust.* **2008**, *80*, 119–132. [CrossRef]
31. Renze, P.; Schröder, W.; Meinke, M. Large-eddy simulation of film cooling flows at density gradients. *Int. J. Heat Fluid Flow* **2008**, *29*, 18–34. [CrossRef]
32. Konopka, M.; Jessen, W.; Meinke, M.; Schröder, W. Large-eddy simulation of film cooling in an adverse pressure gradient flow. *ASME J. Turbomach.* **2013**, *135*, 031031. [CrossRef]
33. Konopka, M.; Meinke, M.; Schröder, W. Large-eddy simulation of high mach number film cooling with shock-wave interaction. *Prog. Flight Phys.* **2013**, *5*, 309–326.
34. Martini, P.; Schulz, A.; Bauer, H.-J.; Whitney, C.F. Detached eddy simulation of film cooling performance on the trailing edge cutback of gas turbine airfoils. *ASME J. Turbomach.* **2006**, *128*, 292–299. [CrossRef]
35. Schneider, H.; von Terzi, D.; Bauer, H.-J. Large-Eddy Simulations of trailing-edge cutback film cooling at low blowing ratio. *Int. J. Heat Fluid Flow* **2010**, *31*, 767–775. [CrossRef]
36. Schneider, H.; von Terzi, D.; Bauer, H.-J. Turbulent heat transfer and large coherent structures in trailing-edge cutback film cooling. *Flow Turbul. Combust.* **2012**, *88*, 101–120. [CrossRef]
37. Schneider, H.; von Terzi, D.; Bauer, H.-J.; Rodi, W. Coherent structures in trailing-edge cooling and the challenge for turbulent heat transfer modelling. *Int. J. Heat Fluid Flow* **2015**, *51*, 110–119. [CrossRef]
38. Rozati, A.; Tafti, D.K. Large-eddy simulations of leading edge film cooling: Analysis of flow structures, effectiveness, and heat transfer coefficient. *Int. J. Heat Fluid Flow* **2008**, *29*, 1–17. [CrossRef]

39. Rozati, A.; Tafti, D.K. Effect of coolant–mainstream blowing ratio on leading edge film cooling flow and heat transfer—LES investigation. *Int. J. Heat Fluid Flow* **2008**, *29*, 857–873. [CrossRef]
40. Rozati, A.; Tafti, D.K. Large eddy simulation of leading edge film cooling—Part II: Heat transfer and effect of blowing ratio. *ASME J. Turbomach.* **2008**, *130*, 041015. [CrossRef]
41. Rozati, A.; Tafti, D.K.; Sreedharan, S.S. Effects of syngas ash particle size on deposition and erosion of a film cooled leading edge. *ASME J. Turbomach.* **2011**, *133*, 011010. [CrossRef]
42. Ziefle, J.; Kleiser, L. Assessment of a film-cooling flow structure by large-eddy simulation. *J. Turbul.* **2008**, *9*, 1–25. [CrossRef]
43. Gräf, L.; Kleiser, L. Large-eddy simulation of double-row compound-angle film cooling: Setup and validation. *Comput. Fluids* **2011**, *43*, 58–67. [CrossRef]
44. Ziefle, J.; Kleiser, L. Numerical investigation of a film-cooling flow structure: Effect of crossflow turbulence. *ASME J. Turbomach.* **2013**, *135*, 041001. [CrossRef]
45. Gräf, L.; Kleiser, L. Film cooling using antikidney vortex pairs: Effect of blowing conditions and yaw angle on cooling and losses. *ASME J. Turbomach.* **2014**, *136*, 011008. [CrossRef]
46. Sakai, E.; Takahashi, T.; Watanabe, H. Large-eddy simulation of an inclined round jet issuing into a crossflow. *Int. J. Heat Mass Transf.* **2014**, *69*, 300–311. [CrossRef]
47. Foroutan, H.; Yavuzkurt, S. Numerical simulations of the near-field region of film cooling jets under high free stream turbulence: Application of RANS and hybrid URANS/large eddy simulation models. *ASME J. Heat Transf.* **2015**, *137*, 011701. [CrossRef]
48. Baek, S.I.; Yavuzkurt, S. Effects of flow oscillations in the mainstream on film cooling. *Inventions* **2018**, *3*, 73. [CrossRef]
49. Yu, F.; Yavuzkurt, S. Near-field simulations of film cooling with a modified DES model. *Inventions* **2020**, *5*, 13. [CrossRef]
50. Al-Zurfi, N.; Turan, A. LES of rotational effects on film cooling effectiveness and heat transfer coefficient in a gas turbine blade with one row of air film injection. *Int. J. Therm. Sci.* **2016**, *99*, 96–112. [CrossRef]
51. Al-Zurfi, N.; Turan, A.; Nasser, A. Numerical investigation of rotation effects on anti-vortex film-cooling holes. *Flow Turbul. Combust.* **2016**, *96*, 133–162. [CrossRef]
52. Al-Zurfi, N.; Nasser, A. LES of rotating film-cooling performance in a 1–1/2 turbine stage. *Propuls. Power Res.* **2019**, *8*, 85–107. [CrossRef]
53. Al-Zurfi, N.; Turan, A.; Nasser, A.; Alhusseny, A. A numerical study of anti-vortex film-cooling holes designs in a 1-1/2 turbine stage using LES. *Propuls. Power Res.* **2019**, *8*, 275–299. [CrossRef]
54. Li, W.; Li, X.; Ren, J.; Jiang, H. Large eddy simulation of compound angle hole film cooling with hole length-to-diameter ratio and internal crossflow orientation effects. *Int. J. Therm. Sci.* **2017**, *121*, 410–423. [CrossRef]
55. Wang, Q.; Su, X.; Yuan, X. Large-eddy simulation of shaped hole film cooling with the influence of cross flow. *Int. J.Turbo Jet Engines* **2020**, 10151520200012.
56. Wang, L.; Li, X.; Ren, J.; Jiang, H. The interaction between upstream and downstream film cooling rows in flow field and heat transfer. *Int. J. Therm. Sci.* **2020**, *149*, 106176. [CrossRef]
57. Wang, C.; Fan, F.; Zhang, J.; Huang, Y.; Feng, H. Large eddy simulation of film cooling flow from converging slot-holes. *Int. J. Therm. Sci.* **2018**, *126*, 238–251. [CrossRef]
58. Wang, C.; Zhang, J.; Feng, H.; Huang, Y. Large eddy simulation of film cooling flow from a fanshaped hole. *Appl. Therm. Eng.* **2018**, *129*, 855–870. [CrossRef]
59. Fan, F.; Wang, C.; Zhang, J. Large eddy simulation of film cooling on turbine vane. *J. Therm. Sci. Tech.* **2019**, *14*, JTST0014. [CrossRef]
60. Wang, C.; Sun, X.; Fan, F.; Zhang, J. Study on trench film cooling on turbine vane by large-eddy simulation. *Num. Heat Transf. Part A Appl.* **2020**, *78*, 338–358. [CrossRef]
61. Huang, K.; Zhang, J.; Wang, C.; Liu, S. Large-eddy simulation of single-row serrated trenched-hole film cooling on turbine guide vane. *Num. Heat Transf. Part A Appl.* **2022**, *81*, 119–141. [CrossRef]
62. Jin, Y.; Lu, L.; Huang, Z.; Han, X. Numerical investigation of flat-plate film cooling using very-large eddy simulation method. *Int. J. Therm. Sci.* **2022**, *171*, 107263. [CrossRef]
63. Stratton, Z.T.; Shih, T.I. Effects of density and blowing ratios on the turbulent structure and effectiveness of film cooling. *ASME J. Turbomach.* **2018**, *140*, 101007. [CrossRef]
64. Milani, P.M.; Gunady, I.E.; Ching, D.S.; Banko, A.J.; Elkins, C.J.; Eaton, J.K. Enriching MRI mean flow data of inclined jets in crossflow with Large Eddy Simulations. *Int. J. Heat Fluid Flow* **2019**, *80*, 108472. [CrossRef]
65. Gunady, I.E.; Milani, P.M.; Banko, A.J.; Elkins, C.J.; Eaton, J.K. Velocity and concentration field measurements and large eddy simulation of a shaped film cooling hole. *Int. J. Heat Fluid Flow* **2021**, *90*, 10883. [CrossRef]
66. Oliver, T.A.; Bogard, D.G.; Moser, R.D. Large eddy simulation of compressible, shaped-hole film cooling. *Int. J. Heat Mass Transf.* **2019**, *140*, 498–517. [CrossRef]
67. Hou, R.; Wen, F.; Luo, Y.; Tang, X.; Wang, S. Large eddy simulation of film cooling flow from round and trenched holes. *Int. J. Heat Mass Transf.* **2019**, *144*, 118631. [CrossRef]
68. Hou, R.; Wen, F.; Wang, S.; Luo, Y.; Tang, X. Large eddy simulation of the trenched film cooling hole with different compound angles and coolant inflow orientation effects. *Appl. Therm. Eng.* **2019**, *163*, 114397. [CrossRef]
69. Zhao, Z.; Wen, F.; Tang, X.; Luo, Y.; Hou, R.; Wang, Z. Large eddy simulation of an inclined jet in crossflow with vortex generators. *Int. J. Heat Mass Transf.* **2021**, *170*, 121032. [CrossRef]

70. Zhao, Z.; Wen, F.; Tang, X.; Song, J.; Wang, Z. Large eddy simulation of pulsed film cooling with vortex generators. *Int. J. Heat Mass Transf.* **2021**, *180*, 12180. [CrossRef]
71. Zhao, Z.; Wen, F.; Tang, X.; Song, J.; Luo, Y.; Wang, Z. Large eddy simulation of film cooling with vortex generators between two consecutive cooling rows. *Int. J. Heat Mass Transf.* **2022**, *182*, 121955. [CrossRef]
72. Zhao, Z.; Wang, S.; Wen, F.; Tang, X.; Song, J.; Wang, Z. Large eddy simulation of compound angle film cooling with vortex generators. *Int. J. Therm. Sci.* **2022**, *178*, 107611. [CrossRef]
73. Baek, S.I.; Ahn, J. Large eddy simulation of film cooling with triple holes: Injectant behavior and adiabatic film-cooling effectiveness. *Processes* **2020**, *8*, 1443. [CrossRef]
74. Baek, S.I.; Ahn, J. Effects of bulk flow pulsations on film cooling with two sister holes. *Appl. Sci.* **2021**, *11*, 1537. [CrossRef]
75. Baek, S.I.; Ryu, J.; Ahn, J. Large eddy simulation of film cooling with forward expansion hole: Comparative study with LES and RANS simulations. *Energies* **2021**, *14*, 2063. [CrossRef]
76. Baek, S.-I.; Ahn, J. Large eddy simulation of film cooling involving compound angle hole with bulk flow pulsation. *Energies* **2021**, *14*, 7659. [CrossRef]
77. Baek, S.-I.; Ahn, J. Effects of bulk flow pulsation on film cooling involving compound angle. *Energies* **2022**, *15*, 2643. [CrossRef]
78. Zamiri, A.; You, S.J.; Chung, J.T. Large eddy simulation of unsteady turbulent flow structures and film-cooling effectiveness in a laidback fan-shaped hole. *Aerosp. Sci. Tech.* **2020**, *100*, 105793. [CrossRef]
79. Zamiri, A.; You, S.J.; Chung, J.T. Large eddy simulation in the optimization of laidback fan-shaped hole geometry to enhance film-cooling performance. *Int. J. Heat Mass Transf.* **2020**, *158*, 120014. [CrossRef]
80. Zamiri, A.; You, S.J.; Chung, J.T. Surface roughness effects on film-cooling effectiveness in a fan-shaped cooling hole. *Aerosp. Sci. Tech.* **2021**, *119*, 107082. [CrossRef]
81. Zamiri, A.; Chung, J.T. Large eddy simulation of compound angle effects on cooling effectiveness and flow structure of fan-shaped holes. *Int. J. Heat Mass Transf.* **2021**, *178*, 121599. [CrossRef]
82. Zamiri, A.; Chung, J.T. Large eddy simulation of internal coolant crossflow orientation effects on film-cooling effectiveness of fan-shaped holes. *Int. J. Heat Mass Transf.* **2022**, *190*, 122778. [CrossRef]
83. Zamiri, A.; Barigozzi, G.; Chung, J.T. Large eddy simulation of film cooling flow from shaped holes with different geometrical parameters. *Int. J. Heat Mass Transf.* **2022**, *196*, 123261. [CrossRef]
84. Chen, X.; Wang, Y.; Long, Y.; Weng, S. Effect of particle deposition on film cooling from fan-shaped holes. *Int. J. Heat Mass Transf.* **2021**, *181*, 122028. [CrossRef]
85. Chen, X.; Wang, Y.; Long, Y.; Weng, S. Effect of partial blockage on flow and heat transfer of film cooling with cylindrical and fan-shaped holes. *Int. J. Therm. Sci.* **2021**, *164*, 106866. [CrossRef]
86. Chen, X.; Long, Y.; Wang, Y.; Weng, S.; Luan, Y. Large eddy simulation of film cooling from cylindrical holes partially blocked by CaO-MgO-Al_2O_3-SiO_2. *Int. Comm. Heat Mass Transf.* **2021**, *129*, 105754. [CrossRef]
87. Kang, Y.S.; Rhee, D.-H.; Song, Y.J.; Kwak, J.S. Large Eddy Simulations on film cooling flow behaviors with upstream turbulent boundary layer generated by circular cylinder. *Energies* **2021**, *14*, 7227. [CrossRef]
88. Kang, Y.S.; Jun, S.; Rhee, D. Large eddy simulations on fan shaped film cooling hole with upstream boundary layer turbulence effect generated by trip strip. *ASME J. Thermal Sci. Eng. Appl.* **2022**, *14*, 031006. [CrossRef]
89. Dupuy, D.; Perrot, A.; Odier, N.; Gicquel, L.Y.; Duchaine, F. Boundary-condition models of film-cooling holes for large-eddy simulation of turbine vanes. *Int. J. Heat Mass Transf.* **2021**, *166*, 120763. [CrossRef]
90. Liess, C. Experimental investigation of film cooling with ejection from a row of holes for the application to gas turbine blades. *ASME J. Eng. Power* **1975**, *97*, 21–27. [CrossRef]
91. Tabor, G.R.; Baba-Ahmadi, M.H. Inlet conditions for large eddy simulation: A review. *Comput. Fluids* **2010**, *39*, 553–567. [CrossRef]
92. Xie, B.; Gao, F.; Boudet, J.; Shao, L.; Lu, L. Improved vortex method for large-eddy simulation inflow generation. *Comput. Fluids* **2018**, *168*, 87–100. [CrossRef]
93. Kong, H.; Choi, H.; Lee, J.S. Direct numerical simulation of turbulent thermal boundary layers. *Phys. Fluids* **2000**, *12*, 2555. [CrossRef]
94. Ekkad, S.V.; Han, J.C.; Du, H. Detailed film cooling measurements on a cylindrical leading edge model: Effect of free-stream turbulence and coolant density. *ASME J. Turbomach.* **1998**, *120*, 799–807. [CrossRef]
95. Kong, H.; Choi, H.; Lee, J.S. Dissimilarity between the velocity and temperature fields in a perturbed turbulent thermal boundary layer. *Phys. Fluids* **2001**, *13*, 1466–1479. [CrossRef]
96. Yee, H.C.; Warming, R.F.; Harten, A. Implicit total variation diminishing (TVD) schemes for steady-state calculations. *J. Comput. Phys.* **1985**, *57*, 327–360. [CrossRef]
97. Jiang, G.S.; Shu, C.W. Efficient implementation of weighted ENO schemes. *J. Comput. Phys.* **1996**, *126*, 202–228. [CrossRef]
98. Germano, M.; Piomelli, P.; Moin, P.; Cabot, W.H. A dynamic sub-grid scale eddy viscosity model. *Phys. Fluids* **1991**, *3*, 1760–1765. [CrossRef]
99. Lilly, D.K. A proposed modification of the germano sub-grid scale closure model. *Phys. Fluids* **1992**, *4*, 633–635. [CrossRef]
100. Anderson, R.; Meneveau, C. Effects of the similarity model in finite-difference LES of isotropic turbulence using a Lagrangian dynamic mixed model. *Flow Turbul. Combust.* **1999**, *62*, 201–225. [CrossRef]
101. Stoll, R.; Porté-Agel, F. Large-eddy simulation of the stable atmospheric boundary layer using dynamic models with different averaging schemes. *Bound. Layer Meteorol.* **2008**, *126*, 1–28. [CrossRef]

102. Ducros, F.; Nicoud, F.; Poinsot, T. Wall-adapting local eddy-viscosity models for simulations in complex geometries. In Proceedings of the 6th ICFD Conference on Numerical Methods for Fluid Dynamic, Tblisi, Georgia, 21–24 June 1998; pp. 293–299.
103. Seo, H.J.; Lee, J.S.; Ligrani, P.M. The effect of injection hole length on film cooling with bulk flow pulsations. *Int. J. Heat Mass Transf.* **1998**, *41*, 3515–3528. [CrossRef]
104. Sinha, A.K.; Bogard, D.G.; Crawford, M.E. Film-cooling effectiveness downstream of a single row of holes with variable density ratio. *ASME J. Turbomach.* **1991**, *113*, 442–449. [CrossRef]
105. Fujimoto, S. Large eddy simulation of film cooling flows using octree hexahedral meshes. In Proceedings of the ASME Turbo Expo 2012, Copenhagen, Denmark, 11–15 June 2012; p. GT2012-70090.
106. Bose, S.T.; Park, G.I. Wall-modeled large-eddy simulation for complex turbulent flows. *Annu. Rev. Fluid Mech.* **2018**, *50*, 535. [CrossRef]
107. Burd, S.W.; Kaszeta, R.W.; Simon, T.W. Measurements in film cooling flows: Hole L/D and turbulence intensity effects. *ASME J. Turbomach.* **1998**, *120*, 791–798. [CrossRef]
108. Jung, I.S.; Ligrani, P.M.; Lee, J.S. Effects of bulk flow pulsations on phase-averaged and time-averaged film-cooled boundary layer flow structure. *ASME J. Fluids Eng.* **2001**, *123*, 559–566. [CrossRef]
109. Schwarz, S.G.; Goldstein, R.J.; Eckert, E.R.G. The influence of curvature on film cooling performance. *ASME J. Turbomach.* **1991**, *113*, 472–478. [CrossRef]
110. Goldstein, R.J.; Eckert, E.R.G.; Burggraf, F. Effects of hole geometry and density on three-dimensional film cooling. *Int. J. Heat Mass Transf.* **1974**, *17*, 595–607. [CrossRef]
111. Sen, B.; Schmidt, D.L.; Bogard, D.G. Film cooling with compound angle holes: Heat transfer. *ASME J. Turbomach.* **1996**, *118*, 800–806. [CrossRef]
112. Gritsch, M.; Schulz, A.; Wittig, S. Effect of internal coolant crossflow on the effectiveness of shaped film-cooling holes. *ASME J. Turbomach.* **2003**, *125*, 547–554. [CrossRef]
113. Cho, H.H.; Rhee, D.H.; Kim, B.G. Enhancement of film cooling performance using a shaped film cooling hole with compound angle injection. *JSME Int. J. Ser. B Fluids Therm. Eng.* **2001**, *44*, 99–110. [CrossRef]
114. Bell, C.M.; Hamakawa, H.; Ligrani, P.M. Film cooling from shaped holes. *ASME J. Heat Transf.* **2000**, *122*, 224–232. [CrossRef]
115. Lee, H.W.; Park, J.J.; Lee, J.S. Flow visualization and film cooling effectiveness measurements around shaped holes with compound angle orientations. *Int. J. Heat Mass Transf.* **2002**, *45*, 145–156. [CrossRef]
116. Lee, K.D.; Kim, K.Y. Shape optimization of a fan-shaped hole to enhance film-cooling effectiveness. *Int. J. Heat Mass Transf.* **2010**, *53*, 2996–3005. [CrossRef]
117. Lee, K.D.; Kim, K.Y. Surrogate based optimization of a laidback fan-shaped hole for film-cooling. *Int. J. Heat Fluid Flow* **2011**, *32*, 226–238. [CrossRef]
118. Seo, H.J.; Kang, Y.J.; Lee, H.C.; Kwak, J.S.; Park, J.S.; Lee, K.D. Optimization of the configuration of the laidback fan-shaped film cooling hole with a lateral expansion angle of 10 degrees. *Appl. Therm. Eng.* **2019**, *153*, 379–389. [CrossRef]
119. Park, S.H.; Kang, Y.J.; Seo, H.J.; Kwak, J.S.; Kang, Y.S. Experimental optimization of a fan-shaped film cooling hole with 30 degrees-injection angle and 6-hole length-to-diameter ratio. *Int. J. Heat Mass Transf.* **2019**, *144*, 118652. [CrossRef]
120. Wu, H.; Cheng, H.; Li, Y.; Rong, C.; Ding, S. Effects of side hole position and blowing ratio on sister hole film cooling performance in a flat plate. *Appl. Therm. Eng.* **2016**, *93*, 718–730. [CrossRef]
121. Ahn, J.; Jung, I.S.; Lee, J.S. Film cooling from two rows of holes with opposite orientation angles: Injectant behavior and adiabatic film cooling effectiveness. *Int. J. Heat Fluid Flow* **2003**, *24*, 91–99. [CrossRef]
122. Yao, J.; Zhang, K.; Wu, J.; Lei, J.; Fang, Y.; Wright, L.M. An experimental investigation on streamwise distance and density ratio effects on double-jet film-cooling. *Appl. Therm. Eng.* **2019**, *156*, 410–421. [CrossRef]
123. Lu, Y.; Dhungel, A.; Ekkad, S.V.; Bunker, R.S. Effect of trench width and depth on film cooling from cylindrical holes embedded in trenches. *ASME J. Turbomach.* **2009**, *131*, 011003. [CrossRef]
124. Abhari, R.S. Impact of rotor–stator interaction on turbine blade film cooling. *ASME J. Turbomach.* **1996**, *118*, 123–133. [CrossRef]
125. Womack, K.M.; Volino, R.J.; Schultz, M.P. Measurements in film cooling flows with periodic wakes. *ASME J. Turbomach.* **2008**, *130*, 041008. [CrossRef]
126. Mazzoni, M.C.; Klostermeier, C.; Rosic, B. Influence of large wake disturbances shed from the combustor wall on the leading edge film cooling. *ASME J. Eng. Gas Turbines Power* **2014**, *136*, 081503. [CrossRef]
127. Sarkar, S.; Babu, H. Large eddy simulation on the interactions of wake and film-cooling near a leading edge. *ASME J. Turbomach.* **2015**, *137*, 011005. [CrossRef]
128. Saumweber, C.; Schulz, A.; Wittig, S. Free-stream turbulence effects on film cooling with shaped holes. *ASME J. Turbomach.* **2003**, *125*, 65–73. [CrossRef]
129. Ligrani, P.M.; Saumweber, C.; Schulz, A.; Wittig, S. Shock wave–film cooling interactions in transonic flows. *ASME J. Turbomach.* **2001**, *123*, 788–797. [CrossRef]
130. Ligrani, P.M.; Gong, R.; Cuthrell, J.M.; Lee, J.S. Bulk flow pulsations and film cooling—I. Injectant behavior. *Int. J. Heat Mass Transf.* **1996**, *39*, 2271–2282. [CrossRef]
131. Lee, J.S.; Jung, I.S. Effect of bulk flow pulsations on film cooling with compound angle holes. *Int. J. Heat Mass Transf.* **2002**, *45*, 113–123. [CrossRef]

132. Ligrani, P.M.; Williams, W. Effects of an embedded vortex on injectant from a single film-cooling hole in a turbulent boundary layer. *ASME J. Turbomach.* **1990**, *112*, 428–436. [CrossRef]
133. Teekaram, A.J.H.; Forth, C.J.P.; Jones, T.V. The use of foreign gas to simulate the effects of density ratios in film cooling. *ASME J. Turbomach.* **1989**, *111*, 57–62. [CrossRef]
134. Wright, L.M.; McClain, S.T.; Clemenson, M.D. Effect of density ratio on flat plate film cooling with shaped holes using PSP. *ASME J. Turbomach.* **2011**, *133*, 041011. [CrossRef]
135. Hale, C.A.; Plesniak, M.W.; Ramadhyani, S. Film cooling effectiveness for short film cooling holes fed by a narrow plenum. *ASME J. Turbomach.* **2000**, *122*, 553–557. [CrossRef]
136. Oda, Y.; Takeishi, K.; Shimizu, D. Large eddy simulation of film cooling with swirling coolant flow. In Proceedings of the ASME/JSME 2011 8th Thermal Engineering Joint Conference, Honolulu, HI, USA, 13–17 March 2011; p. T10102.
137. Kohli, A.; Bogard, D.G. Turbulent transport in film cooling flows. *ASME J. Heat Transf.* **2005**, *127*, 513–520. [CrossRef]
138. Coletti, F.; Benson, M.J.; Ling, J.; Elkins, C.J.; Eaton, J.K. Turbulent transport in an inclined jet in crossflow. *Int. J. Heat Fluid Flow* **2013**, *43*, 149–160. [CrossRef]
139. Schroeder, R.P.; Thole, K.A. Effect of high freestream turbulence on flowfields of shaped film cooling holes. *ASME J. Turbomach.* **2016**, *138*, 091001. [CrossRef]
140. Schroeder, R.P.; Thole, K.A. Thermal field measurements for a shaped hole at low and high freestream turbulence intensity. *ASME J. Turbomach.* **2017**, *139*, 021012. [CrossRef]
141. Kaszeta, R.; Simon, T. Measurement of eddy diffusivity of momentum in film cooling flows with streamwise injection. *ASME J. Turbomach.* **2000**, *122*, 178–183. [CrossRef]
142. Ling, J.; Ryan, K.J.; Bodart, J.; Eaton, J.K. Analysis of turbulent scalar flux models for a discrete hole film cooling flow. *ASME J. Turbomach.* **2016**, *138*, 011006. [CrossRef]
143. Liu, C.; Zhu, H.; Bai, J. New development of the turbulent Prandtl number models for the computation of film cooling effectiveness. *Int. J. Heat Mass Transf.* **2011**, *54*, 874–886. [CrossRef]
144. Milani, P.M.; Ling, J.; Saez-Mischlich, G.; Bodart, J.; Eaton, J.K. A machine learning approach for determining the turbulent diffusivity in film cooling flows. *ASME J. Turbomach.* **2018**, *140*, 021006. [CrossRef]
145. Milani, P.M.; Ling, J.; Eaton, J.K. Generalization of machine-learned turbulent heat flux models applied to film cooling flows. *ASME J. Turbomach.* **2020**, *142*, 011007. [CrossRef]
146. Jung, I.S.; Lee, J.S.; Ligrani, P.M. Effects of bulk flow pulsations on film cooling with compound angle holes: Heat transfer coefficient ratio and heat flux ratio. *ASME J. Turbomach.* **2002**, *124*, 142–151. [CrossRef]